Journal of Neuro-Oncology (2005)
DOI 10.1007/s11060-005-7698-8

Clinical Study

Initial experiences of palliative stereotactic radiosurgery for recurrent brain lymphomas

Masato Sakamoto[1], Natsuo Oya[1,3], Takashi Mizowaki[1], Norio Araki[1], Yasushi Nagata[1], Kenji Takayama[1], Jun A Takahashi[2], Hideyuki Kano[2], Takahisa Katsuki[2], Nobuo Hashimioto[2] and Masahiro Hiraoka[1]
[1]*Department of Radiation Oncology and Image-applied Therapy, Kyoto University Graduate School of Medicine;* [2]*Department of Neurosurgery, Kyoto University Graduate School of Medicine;* [3]*Department of Radiation Oncology, Graduate School of Medical Science, Kumamoto University, Japan*

Key words: chemotherapy, recurrent PCNSL, salvage treatment, SRS, symptomatic relief, toxicity

Summary

In Kyoto University Hospital, stereotactic radiosurgery (SRS) has been performed for its rapid palliative effect in patients with recurrent primary central nervous system lymphoma (PCNSL), often in combination with salvage chemotherapy. In the present study, the treatment outcome and toxicity of SRS for recurrent PCNSL was retrospectively evaluated. Between March 1998 and June 2004, 17 histologically proven recurrent PCNSLs in nine patients were treated with linac-based stereotactic radiosurgery. All patients had developed intracranial recurrences after initial treatment including external beam radiation therapy (EBRT). The prescribed dose was 10.0–16.0 (median 12.0) Gy. Seven of nine patients received systemic chemotherapy around the time of SRS. The target volume was 0.4–24.5 ml (median 3.5 ml). Initial tumor response could be evaluated in 15 of 17 lesions. Among them, radiological complete response (CR), partial response (PR), stable disease (SD) and progressive disease (PD) was observed in 3, 10, 2, and 0 lesions, respectively. One-year overall survival rate and relapse-free survival rate after first SRS was 58% and 22%, respectively. Improvement of symptoms was observed in six patients. The time from SRS to symptomatic relief was 1–57 days (median 3 days). No ≥ grade 2 acute toxicities related to SRS were observed. In conclusion, linac-based SRS with a prescription dose of 10–12 Gy for recurrent PCNSL is useful for palliation, especially considering the short time, rapid tumor response, and low treatment toxicity.

Introduction

Primary central nervous system lymphoma (PCNSL) is a rare brain tumor entity, which accounts for 0.5–1.5% of primary intracranial neoplasms in immunocompetent individuals [1]. The natural course of untreated PCNSL is highly aggressive and fatal, with a median survival time of approximately 1.5–4 months from the time of diagnosis [2–4].

Usually, PCNSL is treated with external beam radiotherapy (EBRT) and/or chemotherapy as an initial treatment, since the radio- and chemosensitivity of PCNSL seems to be as high as that of nodal or extranodal malignant lymphomas that occur in the body. Various combined regimens such as EBRT alone [5,6], EBRT followed by CHOP-like chemotherapy [7,8], high dose intravenous methotrexate alone [9], and high dose methotrexate followed by EBRT [10–12] have been employed, showing a median survival time of 12–30 months [4–12].

Although rapid and complete tumor regression is commonly seen in most cases of PCNSL, intracranial recurrence is often observed even within the previous radiation field. Failure after initial treatment was reported in 35–60% of adequately treated patients with PCNSL [6,13–15].

The prognosis of intracranial recurrent PCNSL seems to be dismal. The median survival time has been reported to be only 2–4 months from the time of recurrence without any treatment. Patients with intracranial recurrent PCNSL may be able to be salvaged with systemic chemotherapy, and possibly with radiotherapy. Several previous reports have shown the effect of these salvage therapies on patient prognosis. Median survival time was reported to be 10–16.5 months [14–16].

The use of conventional EBRT for recurrent PCNSL is often limited in consideration of the tolerance dose of brain parenchyma. In most cases, a large volume of brain parenchyma has been irradiated as a major part of the standard initial therapy. On the other hand, stereotactic radiosurgery (SRS), which has been widely used in the treatment of various brain tumors, may be a treatment option for recurrent PCNSL. Stereotactic irradiation minimizes the irradiated volume of surrounding normal brain parenchyma. This technique delivers an effective radiation dose to the recurrent tumor without severe neurological toxicity, even when the recurrent tumor is located within the field of previous EBRT. However, the microscopic tumor infiltration is not covered by SRS alone.

In our institute, SRS has been performed for its rapid palliative effect in patients with recurrent PCNSL, often in combination with salvage chemotherapy. In the present study, the treatment outcome and toxicity of SRS for recurrent PCNSL was retrospectively evaluated.

Methods and Materials

Patient Background

Between March 1998 and June 2004, 17 histologically proven recurrent PCNSLs in nine patients were treated with linac-based stereotactic radiosurgery at Kyoto University Hospital. There were five male and four female patients and their age was 51–79 (median 66) years old at the time of the first SRS.

All patients had developed intracranial recurrences after initial treatment, including EBRT. The primary tumor lesions had received 37.8–56.0 (median 54.0) Gy using a daily dose of 1.5–2.0 Gy, in which a whole brain irradiation dose of 33.0–48.6 (median 41.4) Gy had been followed by local boost irradiation. The interval between previous EBRT and the first SRS was 6.6–50.4 (median 16.6) months.

Treatment

Corticosteroids were administered to all patients before SRS. Seven of the nine patients received systemic chemotherapy around SRS, including VEPA (vincristin, cyclophosphamide, prednisolone, adriamycin) and DeVIC (dexamethasone, etoposide, ifosfamide, carboplatin) regimens.

All patients underwent SRS using 6 MV X-ray beams generated by Clinac-2300c linear accelerator (Varian Inc., Palo Alto, CA). Treatment planning was carried out using the X-Knife system (Radionics Inc., Burlington, MA), following a 3 mm-slice contrast-enhanced CT scan and MR-CT fusion if necessary. The contrast-enhanced tumor lesions and critical structures, such as eyes, brain stem and optic nerves, were delineated. Planned target volume (PTV) was determined as the contrast-enhanced tumor with a 2–3 mm margin. Four to six beam arcs were arranged first automatically and then manually, so that the optimal dose distribution could be achieved, considering both the doses of PTV and critical structures. Irradiation was carried out in a single fraction. The prescription dose varied according to the tumor size and location. The mean prescribed dose (80% isodose) to PTV was 10.0–16.0 (median 12.0) Gy. One lesion was treated by the combination of two isocenters.

At the time of the first SRS, the number of treated tumors was one for seven patients and two for two patients. Two of the nine patients received multiple SRS sessions at the diagnosis of intracranial distant recurrences following preceding SRS; one patient received the second SRS 27 months after the first SRS, and the other received four sessions of SRS to six tumors during seven months for repeated intracranial distant recurrences.

Outcome evaluation

The patients were followed up with MRI/CT studies. Initial tumor response was evaluated within two months after SRS. In the assessment of the initial tumor response, complete response (CR), partial response (PR), progressive disease (PD), and stable disease (SD) was defined as complete disappearance of the tumor, a $\geq$ 50% reduction in the tumor volume, a $\geq$ 25% increase in the tumor volume, and non-CR/PR and non-PD, respectively.

Intracranial relapse-free survival and overall survival times were calculated from the day of the first SRS using the Kaplan–Meier method. Toxicity was judged by NCI-CTC version 2 criteria.

Neurological status of the patients was evaluated by regular interviews and physical examinations, and scored according to the RTOG functional neurological scale [17].

Results

Treatment parameters

The target volume was 0.4–24.5 (median 3.5) ml. The collimator size used was 12.5–40 (median 30) mm in diameter, and the total beam arc was 160–410 (median 395) in degree. The coverage rate of the prescription dose to PTV was 92–100 (median 99)%. The minimal and maximal tumor dose was 5.5–17.7 (median 9.1) Gy and 12.5–20.3 (median 15.2) Gy, respectively. Major treatment parameters for the 17 tumors are summarized in Table 1. In all cases, the doses to eyes, optic nerves and brain stem did not exceed 12 Gy.

Initial tumor response and local regrowth after SRS

Initial tumor response could be evaluated in 15 of 17 lesions. Among them, radiological CR, PR, SD and PD were observed in 3, 10, 2 and 0 lesions, respectively, as listed in Table 2. The overall response rate (CR plus PR) was 87%. There was no relationship between the initial tumor response and the SRS parameters, including prescription dose, minimal dose, target volume, and the coverage rate. In Figure 1, an example of CR is shown.

Local tumor regrowth was seen in one lesion, which had received a prescription dose of 12.0 Gy and a minimal dose of 6.4 Gy. It was initially judged PR, but increased in size 2.4 months after SRS.

Pattern of recurrence after SRS and survival

One patient remained disease-free for 20.3 months, one patient developed local regrowth 2.4 months after SRS, and seven patients developed intracranial distant recurrences 0.7–27.2 (median 3.1) months after the first SRS. Recurrences after the first SRS were salvaged by further SRS in two patients, and by systemic chemotherapy in three patients.

One-year overall survival rate and one-year intracranial relapse-free survival rate was 58% and 22%, respectively, as shown in Figure 2. Median overall survival time and median intracranial relapse-free survival time was 7.7 months and 3.7 months, respectively. No relationship between the SRS parameters and survival was observed in the present study. However, the median overall survival time in patients with peri-SRS chemotherapy was significantly longer than that in patients

Table 1. Patient characteristic and treatment parameter of SRS

Patients	Sex	Lesion number	Location	Age at SRS (y.o.)	Time between EBRT and SRS (month)	Lesion volume (ml)	Isocenter/Prescription dose (Gy)	Max / Min dose (Gy)
1	F	1	lt. Frontal lobe	57	16.6	9.4	20.0 / 16.0	20.3 / 17.7
2	M	1	rt. Thalamus	62	29.1	5.3	15.0 / 12.0	15.8 / 12.7
		2	lt. Internal capsule	62	29.1	1.0	15.0 / 12.0	17.4 / 11.6
3	M	1	lt. Temporo-occipital lobe	66	50.4	7.8	15.0 / 12.0	15.3 / 13.5
4	F	1	rt. Parietal lobe	64	33.8	18.5	15.0 / 12.0	15.2 / 6.4
5	M	1	rt. Frontal lobe	79	10.2	1.8	15.0 / 12.0	15.0 / 12.9
6	F	1	Cerebellum	67	6.6	14.6	15.0 / 12.0	17.5 / 7.8
7	F	1	rt. Lateral ventricle	71	16.6	1.1	15.0 / 12.0	15.0 / 13.6
		2	lt. Occipital lobe	73	43.9	4.9	15.0 / 12.0	15.3 / 13.8
8	M	1	rt. Frontal lobe	51	12.8	14.9	12.5 / 10.0	13.0 / 5.5
		2	Brain stem	51	12.8	24.5	12.5 / 10.0	15.6 / 6.4
9	M	1	rt. Insula	69	37.1	2.7	15.0 / 12.0	15.0 / 7.1
		2	rt. Temporal lobe	69	38.4	1.8	15.0 / 12.0	15.0 / 12.3
		3	lt. Occipital lobe	69	38.4	0.4	15.0 / 12.0	15.2 / 9.0
		4	lt. Lateral ventricle	69	39.4	2.3	12.5 / 10.0	12.5 / 9.1
		5	rt. Basal ganglia	69	41.6	3.5	12.5 / 10.0	12.9 / 7.9
		6	Fourth ventricle	69	41.6	0.4	12.5 / 10.0	12.9 / 7.4

without peri-SRS chemotherapy (5.9 vs. 13.0 months, $P = 0.046$), as shown in Figure 3.

Palliative effects

Eight of the nine patients had symptoms possibly resulting from recurrent tumors before the first SRS. For six of these patients, symptomatic relief was achieved; in five patients the motor function was improved, and in the other patient the frequency of convulsion was remarkably decreased.

Comparing the scores in the RTOG functional neurological scale before and after the first SRS, improvement in the neurological status was observed in five of the nine patients, as shown in Table 2.

The time from SRS to symptomatic relief was 1–57 (median 3) days.

Toxicity

No ≥ grade 2 acute toxicities related to SRS were observed, although three of the nine patients developed grade 3 bone marrow toxicity due to peri-SRS systemic chemotherapy.

Discussion

The role of SRS in the treatment of PCNSL has not been established. In several institutions, SRS is often

Table 2. Treatment results of SRS (Initial tumor response and symptomatic improvement)

Patients	Sex	Lesion number	Location	Initial tumor response	Symptomatic improvement after first SRS	Functional neurological level change	Survival time after first SRS (month)
1	F	1	lt. Frontal lobe	PR	(+) decreasing frequency of convulsions	4 → 4	6.6
2	M	1	rt. Thalamus	SD	(–)	4 → 4	14.9
		2	lt. Internal capsule	SD			
3	M	1	lt. Temporo-occipital lobe	PR	(+) improving gait disturbance and disorientation	1 → 0	20.3
4	F	1	rt. Parietal lobe	PR	(+) improving gait disturbance	4 → 3	5.5
5	M	1	rt. Frontal lobe	CR	(+) improving gait disturbance and eye movement	3 → 2	6.3
6	F	1	Cerebellum	CR	(–)	4 → 4	2.1
7	F	1	rt. Lateral ventricle	CR	(+) improving results of MMT	2 → 1	47.8
		2	lt. Occipital lobe	PR			
8	M	1	rt. Frontal lobe	PR	(+) improving eye movement, diplopia and gait disturbance	2 → 1	13.0
		2	Brain stem	PR			
9	M	1	rt. Insula	PR	(–)	0 → 0	7.7
		2	rt. Temporal lobe	PR			
		3	lt. Occipital lobe	PR			
		4	lt. Lateral ventricle	PR			
		5	rt. Basal ganglia	?			
		6	Fourth ventricle	?			

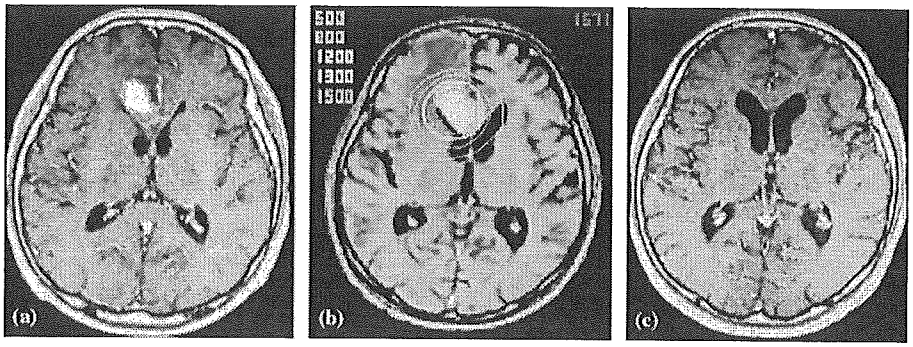

Figure 1. A case with recurrent PCNSL treated with SRS. A 51-year-old man with multiple intracranial recurrent tumors approximately one year after initial treatment. At first, several courses of salvage chemotherapy were attempted, but two of the tumors were resistant to chemotherapy (rt. frontal lobe and brain stem). Cranial nerve palsy and gait disturbance were progressive. Palliative SRS was performed at a prescription dose of 10 Gy. (a) MR image at the time of SRS, (b) treatment planning, (c) MR image three months after SRS.

performed in the initial treatment of newly diagnosed PCNSL, when strong and rapid localized effects are expected. For elderly patients with PCNSL, for whom EBRT or chemotherapy cannot be safely performed, SRS alone may be indicated as a treatment option [11,18]. However, considering the dose distribution character of SRS and the infiltrative and intracranial migration-prone nature of PCNSL, SRS has been generally used as part of the initial treatment combined with EBRT and/or chemotherapy, if treated with curative intent [15,16,19].

In other institutions, SRS for PCNSL has been mainly performed for palliation. In our institution, newly diagnosed PCNSL is usually treated with chemotherapy followed by EBRT, and recurrent PCNSL is treated with SRS with or without chemotherapy, in patients with symptomatic intracranial recurrence, whose neurological symptoms may be improved by tumor volume reduction. So far, however, only a few previous papers have shown the outcome of SRS in this use. Therefore, we evaluated the treatment effects and toxicity of SRS for recurrent PCNSL and reported our initial experiences.

Recurrent brain tumors, including gliomas, meningiomas, and metastatic brain tumors, are also treated with SRS, when they recurred after full dose EBRT. However, in most cases, a relatively high SRS dose is required to achieve tumor regression and/or symptomatic improvement [20–23]. On the other hand, it is expected that recurrent PCNSL remains radiosensitive, compared with the other recurrent brain tumor entities. In the present study, a prompt and drastic response even to a lower SRS dose was demonstrated.

With respect to the SRS dose, 18–24 Gy (as the isocenter dose of stereotactic radiotherapy) [11] and 12.5–23 Gy (as the marginal dose of gamma-knife) [18] were used in the previous reports. The prescription dose of 10–12 Gy used in the present series seems to be adequate for recurrent PCNSL, considering that all of the 17 lesions, except two lesions in patient 2, showed tumor regression. In addition, no SRS-related toxicity was observed, suggesting that an SRS dose of 10–12 Gy could be safely given after a full dose of EBRT, even for patients with recurrent PCNSL adjacent to the brain stem or optic nerves.

In the present series, only one large tumor lesion in patient 4 developed local regrowth. The tumor volume of this lesion was 18.5 ml at the time of SRS, and the minimum dose was as low as 6.4 Gy, while the prescription dose (12 Gy) coverage was 97%. This lesion once showed tumor regression associated with good palliative effects, but developed local regrowth 2.4 months after SRS. Although the focus of tumor regrowth could not be identified, it was probable that the existence of a small part of the tumor irradiated with an

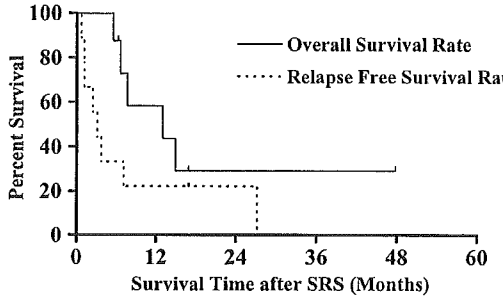

Figure 2. Graph showing Kaplan–Meier estimate of overall survival rate (——) and relapse-free survival rate (- - - -) in all patients after the first SRS for recurrent PCNSL (median survival, 7.7 and 3.3 months, respectively).

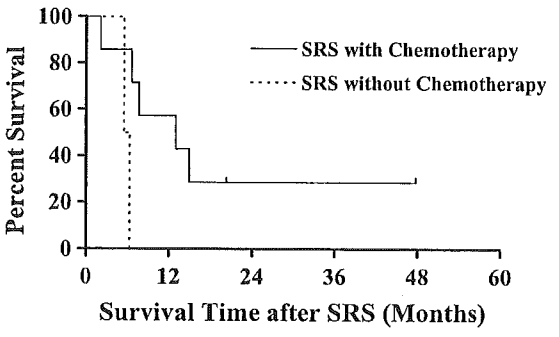

Figure 3. Graph showing Kaplan–Meier estimate of survival rate comparison after the first SRS for recurrent PCNSL between the patients treated SRS with chemotherapy (——, n = 7) versus the patients treated SRS without chemotherapy (- - - -,n = 2). Median overall survival was longer in the SRS with chemotherapy cohort (13.0 months) than the SRS without chemotherapy cohort (5.9 months) (P = 0.046).

insufficient dose might have resulted in the local regrowth.

Symptomatic relief was achieved in six of eight cases, as expected, which demonstrated the excellent usefulness of SRS as a palliative indication. In addition, a considerably prompt response (median 3 days) should be noted as an advantage of SRS.

With respect to the survival time, one-year- and two-year-survival after the first SRS, were 58% and 22%, respectively, and the median survival time after the first SRS was 7.7 months in all patients and 13.6 months in the patients treated with chemotherapy in the present series. These results were slightly inferior to those of the salvage treatments using systemic chemotherapy and/or radiation therapy for recurrent PCNSL in a previous report, in which the median survival time was reported to be 14 months [14,15]. Considering the expected lifetime of only 2–4 months for patients with non-treated recurrent PCNSL [14,15], the results in the present series also demonstrated the survival benefit of SRS in patients with recurrent PCNSL.

Various regimens of systemic chemotherapy are often chosen for patients with recurrent PCNSL. Several previous reports have shown promising treatment response [16,24–26].

Arellano-Rodrigo et al. [16] reported that CR was obtained in six of sixteen cases (37%) and one-year survival was 41% with etoposide, ifosfamide, and cytarabine treatment. However, toxicity consisted of neutropenic fever in 50% of cases, including three cases of sepsis and two cases of pneumonia. In addition, severe encephalopathy was observed in one case. Soussain et al. [24] reported the results of a phase II study of 22 patients treated with intensive chemotherapy with hematopoietic stem-cell rescue. In that study, an objective response was seen in 82%, and the overall three year survival was 64%. On the other hand, after intensive chemotherapy with hematopoietic stem-cell rescue, all patients had grade 4 neutropenia and grade 4 thrombocytopenia. In addition, there was possibility that five of seven patients $\geqslant$ 60 years of age died from treatment complications. Reni et al. [25] reported the results that median survival for all patients was 3.5 months (range 0.4–43 months). One year overall survival was 38%. There were five CR in 23 evaluable patients. But CR occurred after two cycles of temozolomide in four patients and after ten cycles in one patient. Three CR patients received four cycles of temozolomide, one patient eight cycles and one patient twelve cycles. Enting et al. [26] reported the treatment outcome with rituximab and temozolomide as a 53% response rate, median overall survival of 14 months, and median progression free survival of 7.7 months, while there was a 20–30% grade 3 hematologic toxicity (in 15 patients, grade 3 thrombocytopenia was seen in four patients, grade 3 anemia in one and grade 3 leukopenia in one).

It is difficult to compare simply the treatment outcome of chemotherapy and that of SRS, because the treatment modality is usually selected according to the tumor size, location and distribution in individual patients. However, particularly for palliative indication, SRS seems to have several advantages over systemic chemotherapy, even though the contribution of SRS to the survival benefit was not revealed clearly in the present study. First, the treatment time of SRS, usually a couple of days, is much shorter than that of effective chemotherapy, which requires several days or weeks. Second, more prompt symptomatic relief may be expected by SRS compared with chemotherapy. Third, SRS is usually performed without systemic toxicity, including hematological toxicity, which may potentially prolong the time of hospitalization. Therefore, SRS is suited for the palliative intent, if it is expected that volume reduction of recurrent PCNSL may provide symptomatic relief.

In patients with a good prognosis, combination of SRS and systemic chemotherapy seems to be indicated. In the present study, six out of nine patients received chemotherapy. The median survival time of the six patients was longer than that of the three patients treated with SRS alone, although there was treatment selection bias.

In conclusion, *linac*-based SRS with a prescription dose of 10–12 Gy for recurrent PCNSL is useful for palliation, especially considering the short treatment time, rapid tumor response, and low treatment-related toxicity. Although the survival benefit of SRS for recurrent PCNSL was unclear, the combination of SRS and chemotherapy may be an effective strategy for better clinical outcome. This optimal treatment regimen of combined therapy for recurrent PCNSL should be established.

References

1. Fine HA, Mayer RJ: Primary central nervous system lymphoma. Ann Intern Med 119: 1093–1104, 1993
2. Plotkin SR, Batchelor TT: Primary nervous-system lymphoma. Lancet Oncol 2: 354–365, 2001
3. Ferreri AJ, Abrey LE, Blay JY, Borisch B, Hochman J, Neuwelt EA, Yahalom J, Zucca E, Cavalli F, Armitage J, Batchelor T: Summary statement on primary central nervous system lymphomas from the Eighth International Conference on Malignant Lymphoma, Lugano, Switzerland, June 12 to 15, 2002. J Clin Oncol 21: 2407–2414, 2003
4. van der Sanden GA, Schouten LJ, van Dijck JA, van Andel JP, van der Maazen RW, Coebergh JW, Working Group of Specialists in Neuro-Oncology in the Southern, Eastern Netherlands: Primary central nervous system lymphomas: incidence and survival in the Southern and Eastern Netherlands. Cancer 94: 1548–1556, 2002
5. Ishikawa H, Hasegawa M, Tamaki Y, Hayakawa K, Akimoto T, Sakurai H, Mitsuhashi N, Niibe H, Tamura M, Nakano T: Comparable outcomes of radiation therapy without high-dose methotrexate for patients with primary central nervous system lymphoma. Jpn J Clin Oncol 33: 443–449, 2003
6. Shibamoto Y, Tsuchida E, Seki K, Oya N, Hasegawa M, Toda Y, Takemoto M, Sumi M, Hiratsuka J, Oguchi M, Hosono M, Yasuda S, Sougawa M, Kakutoh Y, Hayabuchi N: Primary central nervous system lymphoma in Japan 1995–1999: changes from the preceding 10 years. J Cancer Res Clin Oncol 130: 351–356, 2004
7. Bessell EM, Lopez-Guillermo A, Villa S, Verger E, Nomdedeu B, Petit J, Byrne P, Montserrat E, Graus F: Importance of radiotherapy in the outcome of patients with primary CNS lymphoma: an analysis of the CHOD/BVAM regimen followed by two different radiotherapy treatments. J Clin Oncol 20: 231–236, 2001

8. Bessell EM, Graus F, Lopez-Guillermo A, Villa S, Verger E, Petit J, Holland I, Byrne P: CHOD/BVAM regimen plus radiotherapy in patients with primary CNS non-Hodgkin's lymphoma. Int J Radiat Oncol Biol Phys 50: 457–464, 2001
9. Cheng T, Forsyth P, Chaudhry A, Morris D, Gluck S, Russell JA, Stewart DA: High-dose thiotepa, busulfan, cyclophosphamide and ASCT without whole-brain radiotherapy for poor prognosis primary CNS lymphoma. Bone Marrow Transplant 31: 679–685, 2003
10. Poortmans PM, Kluin-Nelemans HC, Haaxma-Reiche H, Van't Veer M, Hansen M, Soubeyran P, Taphoorn M, Thomas J, Van den Bent M, Fickers M, Van Imhoff G, Rozewicz C, Teodorovic I, van Glabbeke M, European Organization for Research, Treatment of Cancer Lymphoma Group: High-dose methotrexate-based chemotherapy followed by consolidating radiotherapy in non-AIDS-related primary central nervous system lymphoma: European Organization for Research and Treatment of Cancer Lymphoma Group Phase II Trial 20962. J Clin Oncol 21: 4483–4488, 2003
11. Watanabe T, Katayama Y, Yoshino A, Komine C, Yokoyama T, Fukushima T: Long-term remission of primary central nervous system lymphoma by intensified methotrexate chemotherapy. J Neurooncol 63: 87–95, 2003
12. Plasswilm L, Herrlinger U, Korfel A, Weller M, Kuker W, Kanz L, Thiel E, Bamberg M: Primary central nervous system (CNS) lymphoma in immunocompetent patients. Ann Hematol 81: 415–423, 2002
13. Shibamoto Y, Hayabuchi N, Hiratsuka J, Tokumaru S, Shirato H, Sougawa M, Oya N, Uematsu Y, Hiraoka M: Is whole-brain irradiation necessary for primary central nervous system lymphoma? Patterns of recurrence after partial-brain irradiation. Cancer 97: 128–133, 2003
14. Reni M, Ferreri AJ, Villa E: Second-line treatment for primary central nervous system lymphoma. Br J Cancer 79: 530–534, 1999
15. Reni M, Ferreri AJ: Therapeutic management of refractory or relapsed primary central nervous system lymphomas. Ann Hematol 80(Suppl 3): B113–117, 2001
16. Arellano-Rodrigo E, Lopez-Guillermo A, Bessell EM, Nomdedeu B, Montserrat E, Graus F: Salvage treatment with etoposide (VP-16), ifosfamide and cytarabine (Ara-C) for patients with recurrent primary central nervous system lymphoma. Eur J Haematol 70: 219–224, 2003
17. Radiation Therapy Oncology Group: RTOG 95-07 Phase I Study OF Topotecan Plus Cranial Radiation for Glioblastoma Multiforme (NSC #609699) Appendix II Neurologic Function (NF) Status
18. Dong Y, Pan L, Wang B, Wang E, Zhang N, Cai P, Dai J: Stereotactic radiosurgery in the treatment of primary central nervous system lymphoma. Chin Med J (Engl) 116: 1166–1170, 2003
19. Tyson RM, Siegal T, Doolittle ND, Lacy C, Kraemer DF, Neutwelt EA: Current status and future of relapsed primary central nervous system lymphoma (PCNSL). Leuk Lymphoma 44: 627–633, 2003
20. Stafford SL, Pollock BE, Foote RL, Gorman DA, Nelson DF, Schomberg PJ: Stereotactic radiosurgery for recurrent ependymoma. Cancer 88: 870–875, 2000
21. Hudes RS, Corn BW, Werner-Wasik M, Andrews D, Rosenstock J, Thoron L, Downes B, Curran WJ Jr: A phase I dose escalation study of hypofractionated stereotactic radiotherapy as salvage therapy for persistent or recurrent malignant glioma. Int J Radiat Oncol Biol Phys 43: 293–298, 1999
22. Alexander E III, Loeffler JS: Radiosurgery for primary malignant brain tumors. Semin Surg Oncol 14: 43–52, 1998
23. Varlotto JM, Flickinger JC, Niranjan A, Bhatnagar AK, Kondziolka D, Lunsford LD: Analysis of tumor control and toxicity in patients who have survived at least one year after radiosurgery for brain metastases. Int J Radiat Oncol Biol Phys 57: 452–464, 2003
24. Soussain C, Suzan F, Hoang-Xuan K, Cassoux N, Levy V, Azar N, Belanger C, Achour E, Ribrag V, Gerber S, Delattre JY, Leblond V: Results of intensive chemotherapy followed by hematopoietic stem-cell rescue in 22 patients with refractory or recurrent primary CNS lymphoma or intraocular lymphoma. J Clin Oncol 19: 742–749, 2001
25. Reni M, Mason W, Zaja F, Perry J, Franceschi E, Bernardi D, Dell'Oro S, Stelitano C, Candela M, Abbadessa A, Pace A, Bordonaro R, Latte G, Villa E, Ferreri AJ: Salvage chemotherapy with temozolomide in primary CNS lymphomas: preliminary results of a phase II trial. Eur J Cancer 40: 1682–1688, 2004
26. Enting RH, Demopoulos A, DeAngelis LM, Abrey LE: Salvage therapy for primary CNS lymphoma with a combination of rituximab and temozolomide. Neurology 63: 901–903, 2004

Address for offprints: Masato Sakamoto, M.D., Department of Radiation Oncology and Image-applied Therapy, Kyoto University Graduate School of Medicine, 54 Shogoin-Kawaharacho Sakyo-ku, Kyoto, Japan; Tel: +81-75-751-3419; Fax: +81-75-771-9749; E-mail: skmt@kuhp.kyoto-u.ac.jp

Dosimetric properties of the liquid ionization chamber electronic portal imaging device (EPID)

[1] *Radiation Oncology, Imaging and Diagnosis, Molecular and Organ Regulation, Sapporo Medical University, Graduate School of Medicine*

[2] *Division of Radiology and Nuclear Medicine, Sapporo Medical University Hospital, School of Medicine*

[3] *Department of Radiology, Sapporo Medical University, School of Medicine*

[4] *Department of Radioisotope Research, Sapporo Medical University, School of Medicine Biomedical Research, Education and Instrumentation Center*

Kunihiko Tateoka [1) 2)] Atushi Oouchi,[3)] Masaaki Waka,[4)] Kensei Nakata,[3)] Daiki Nagase,[2)] Kazunari Shimizume,[2)] Tunehiko Saikawa,[2)] and Masato Hareyama[1,2,3)]

Abstract

In the relation between the pixel values of the electronic portal imaging device (EPID) and dose rate, pixel values have been reported to be proportional to the square roots of the dose rates although some researchers have reported that each EPID pixel value was almost proportional to the dose rates when they were more than 1 Gy/min. To resolve this contradiction, in this study we have investigated the dosimetric properties of the liquid ionization chamber EPID based on a two-dimensional matrix of liquid-filled ionization chambers. Our results show that the pixel values of this EPID were proportional to the square roots of the dose rates when they were less than 0.5 Gy/min, and the values were proportional to the dose rates when they were more than that. In addition, the survival time of electrons in the liquid of the EPID is reportedly dependent on the amount of impurities in the liquid ionizing chamber of EPID. The pixel values of the EPID acquired in rapid succession, increased. In the results, the pixel values were constantly increased to approximately 0.2% of pre-images for less than 15 s of the rest interval. When changes in the sensitivity of each pixel value were approximately 1%, approximately 5% changes were observed against the transformed dose rate. To avoid this difference, we developed the following formula relating the pixel value, P, and dose rate, D.

$$P = a \cdot D + b \cdot \sqrt{D} - k \cdot h$$

(a, b, h: constants, k: variable)

Received Dec.21, 2005; revision accepted Feb.10, 2006

I. INTRODUCTION

Radiotherapy has been verified by image verification, in which portal images are compared visually with simulation images or digitally reconstructed radiographs (DRRs). Image verification has been developed which uses electronic portal imaging devices (EPIDs) that are computer-controlled through an on-line connection with an actuator. Generally, there are three types of EPIDs: a mirror-based video system, a fiber-optic video system, and a liquid ionization chamber system [1]. Although the image collecting methods are different, image verification can be conducted in a short time without interrupting the process of film development to obtain an EPID image on-line[2]. Moreover, dose verification is an essential process in radiotherapy.

Thus far, dose verification has been performed using a thermoluminescent dosimeter (TLD) placed in an anthropomorphic phantom and by measuring the dose that penetrates into the body, by film. However, measurements using TLDs and semiconductor detectors can be done at only a few points simultaneously, and the film method is not satisfactory with respect to clinical applications because of the film development time [3-7].

Recently, studies have been conducted to verify the possibility of using EPID images as a dosimeter to verify the penetrated dose[8-16]. Van Herk[10] indicated that using the liquid ionization chamber EPID, the square roots of dose rates and the EPID signal pixel values were proportional. On the basis of his study, many researchers obtained corrected dose rates from the measured EPID pixel values. However, Essers et al.[8] reported that in the measurement system for an aerial dose rate using a small phantom, dose rates and EPID signals were proportional when dose rates were more than 1 Gy/min. Curtin-Savard and Podgorsak [16] attributed the observation of Essers et al. to the amount of electric charge being constantly increased by contaminants in the isooctane used as an ionization layer of the EPID in the sequential image collection over a short time." Zhu et al.[14] reported that the EPID showed a maximum change of 3% in the sensitivity during 90-day period, and showed a standard deviation within 1.2% as daily changes. Essers et al.[8] suggested that the influence of scattered material included within the EPID could not be ignored. On the other hand, Zhu et al.[14] considered that there is no major effect from scattered material based on the fact that EPID signals were obtained on irradiation fields of various sizes.

However, the relative differences in the amounts of electric charges between EPID dosimetry and conventional dosimetry with a farmer type cylindrical ionization chamber and a solid phantom have not been distinguished.

The purpose of this paper is to elucidate dosimetric properties of the ionization chamber EPID system. We have quantified the fluctuation of the pixel values depending on the image collection conditions and the change in the amount of electric charges due to impurity in the liquid ionization chamber.

Ⅱ. MATERIALS and METHODS

A. Equipment

The liquid ionization chamber EPID (Portal Vision System, Varian Medical System, Palo Alto, CA) used in this study was installed with the linear accelerator (CLINAC2100C, Varian Medical System, Palo Alto, CA) that generated 4 MV and 10 MV. The ionization chamber was sequenced in the matrix of 256 × 256 pixels (total 65536 pixels). The image collection area was 32.5 cm × 32.5 cm. There were two pole boards (printed circuit boards, PCBs) on the upper and lower sides of the ionization layer which was a 1 mm thick isooctane phase. A 1 mm thick layer of barium and plastic material (density: 4.75 g/cm^3) on the upper surface of the PCB functioned as the build-up material of the X-rays. Each pixel was 1.27 mm × 1.27 mm × 1.0 mm. The front and back of the build-up region were approximately 10 mm and 5 mm of water equivalent material, respectively[8-13].

The dosimetric properties were evaluated from the dose determined by using EPID (L-EPID dose) and the values from the farmer type cylindrical ionization chamber (NE2581, NE Technology Ltd., Berkshire, UK). The area of the irradiation field was decided as 10 cm × 10 cm, and source-to-surface distance (SDD) was 100 cm. Tough Water (Kyoto Kagaku Co., Ltd., Kyoto, Japan) was used as a solid phantom for the measurement. The depth for the measurement point at 4 MV and 10 MV was fixed at the depth of dose maximum (dmax) (4 MV: 1.0 cm and 10 MV: 2.5 cm). For the measurement using the farmer type cylindrical ionization chamber, the thickness of Tough Water below the measurement point was prepared as 5 mm to replicate the geometrical arrangement of the image from the EPID.

To confirm build-up area in front of the EPID surface, tissue maximum ratio (TMR) was measured at 4 MV and 10 MV. The EPID pixel values were a maximum value at X-ray energies of 4 MV and 10 MV when Tough Water thickness was adjusted to 3 mm and 18 mm, respectively, and these Tough Water thicknesses were used for the study. To avoid variations in the pixel values, the mean value of 11 x 11 pixels was used as the EPID pixel value on the central axis of the X-ray beam. Variation in the mean values was within approximately 0.5% of the standard deviation. Moreover, to minimize the influence of the variation, we used the average of 10 images which decreased the standard deviations of the changes to 0.2%. The settings of the EPID and the accelerator are shown in Table I. Ionex Dose Master 2590B (NE Technology Ltd., Berkshire, UK) was used as the electrometer.

Table I. EPID conditions for 4 MV X-rays with 250 MU/min and 10 MV X-rays with 240 MU/min .

Energy	4MV	10MV
Dose rate	250 MU/min	240 MU/min
Sync Frequency	400Hz	180Hz
Interpulse Distance	2.50ms	5.56ms
HV Row Cycle Time	12.50ms	11.11ms
number of Pulses Used for on Sync	5pulses	2pulses
number of row per sync pulse	1row	1row
number of Averages (Row Sweeps)	2scans	1scans
Total Acquision time	3.35sec	2.98sec

B. Measurement of dosimetric properties

1. Effect of contaminants on the liquid ionization chamber EPID

Isooctane in the ionization layer of the liquid ionization chamber is known to contain some contaminants. These contaminants may affect the survival time of the electric charge because they delay movement of the electric charge in isooctane[8]. On observing the phenomena, we concluded that the pixel values increase with continued collection during the survival time of the electric charge. To examine the effects of contaminants in isooctane on the pixel values, we measured four series of ten EPID images (groups A, B, C, and D). Each measurement group was comprised of 10 images and their image acquisition interval (rest interval) was 5, 15, 30, and 60 s, respectively. The collection interval between each measured group was 120 s.

2. The dosimetric properties of EPID as reported by Van Herk

As the voltage is supplied to the ionization chamber in L-EPID with the ray pulse of the accelerator, the voltage supply time is shorter than the movement time to the pole of an ion pair generated by the X-ray beam and its survival time. On the other hand, in the measurement used for a conventional ionization chamber, the voltage supply time is longer than the movement time to the pole of an ion and its survival time, because voltage is continuously supplied during the period in which a ray is irradiated as a pulse. It is considered, on the basis of these facts, that the collecting method of ions using EPID is different from that using the conventional ionization chamber.

Van Herk[10] proposed a new theory concerning the collecting method of ions using L-EPID. According to this theory, in each ionization chamber, ion pairs, $n(t)$ are generated by an X-ray beam, and the changing rate, $dn(t)/dt$, against the time $n(t)$ contains two changing rates of positive and negative ions. The total numbers of ion pairs, $N_{in}(t)$ is proportional to the dose rate, D, and to the number of positive ions, $n(t)_+$ and negative ions, $n(t)_-$,because in this case, negative ions imply ion recombination.

On the basis of the consideration mentioned above, the number of ion pairs, $dn(t)/dt$ is given by the following formula,

$$\frac{dn(t)}{dt} = N_{in}(t) - \alpha n(t)^2 \qquad (1)$$

where α is a constant.

However, as with long time irradiation, the generation of new ion pairs balances the loss of ion pairs caused by the ion recombination, the left side of formula (1) becomes zero ($dn(t)/dt = 0$) and $n(t)$ is expected to be $n(t) \equiv n_{eq}$. Therefore, n_{eq} is expressed by formula (2).

$$n_{eq} = \sqrt{\frac{N_{in}}{\alpha}}$$

$$n_{eq} = \sqrt{\frac{\beta}{\alpha} \cdot D} \qquad (2)$$

Here, $N_{in} = \beta \times D$ and β is a constant. According to this formula, the EPID pixel values are proportional to the square root of dose rate.

To confirm the above formula and to examine the relationship between the actual dose and the EPID pixel value, we collected EPID images using 4 MV and 10 MV X-rays while changing the dose rate and while changing the thickness of the lead board on the tray of the accelerator from 0 mm to 80 mm. In addition, under the same conditions, the dose rate was measured with a farmer type cylindrical ionization chamber. On the basis of these results, a characteristic curve for the EPID was obtained.

3. Effect of scattered radiation

An arbitrary ionizing chamber is affected by scatter radiation generated from surrounding EPID ionizing chambers. To evaluate the effect, L-EPID images were collected while changing radiation field sizes from 4 cm × 4 cm to 20 cm × 20 cm. Each image was converted to a dose rate using the characteristic curve and then the dose rates were compared with those measured under identical conditions by the farmer type cylindrical ionization chamber.

Ⅲ. RESULTS

A. Effects of contaminants in the liquid ionization chamber

In the case where image-collecting intervals were below 15 s (measurement Groups A and B), the pixel values increased slightly (approximately 0.06%) in each EPID image. As compared with the initial image, the pixel value of the 10th image increased from approximately 1.0% to 1.3%. When the image-collecting intervals were set at more than 30 s (Groups C and D), the change in the pixel value was within approximately ±0.25% and was stable. These results agreed with

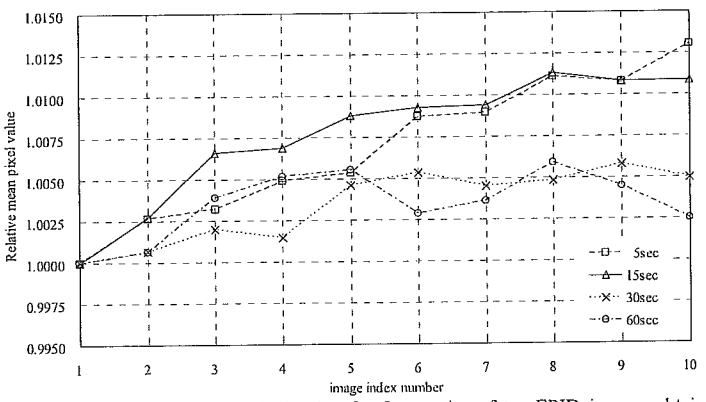

Fig. 1 Reproducibility of mean pixel value for four series of ten EPID images obtained under the same conditions at a 250 MU/min, 100 cm SOD, and 10 cm × 10 cm field size on the central axis at the maximum depth with 4 MV X-rays. The rest intervals between image acquisitions were 5, 15, 30, and 60 s. The region of interest for calculating the mean consisted of 11 × 11 pixels centered on the central field. The mean pixel values were normalized to 1.0 for the first image of each series.

those described by Curtin-Savard and Podgorsak[15].

Moreover, the difference in pixel values between the first image of Group B and that of Group D was approximately 1.6%. On the basis of these results, we decided to use a 30 s interval of image collection (Group C) using the EPID (Fig.1).

B. The dosimetric properties of the EPID

In Fig. 2, pixel value is plotted against the dose rate for each thickness value of the lead board measured with the farmer type cylindrical ionization chamber. The pixel values increased rapidly at a low dose rate, at 4 MV or 10 MV. When the dose rate exceeded 0.5 Gy/min, the pixel values showed a gradual increase.

The pixel values shown in Fig. 2 were calculated on the basis of Van Herk's theory[10] and these calculated values are shown in Fig. 3. The relationship between the pixel values and the square roots of the dose rates was linear, but not a strict one. To elaborate, in the range in which the pixel values increased rapidly against the dose rates, the pixel values showed an approximately proportional increase with the square roots of the dose rates. In the range in which the pixel values showed a gradual increase, the pixel values showed an approximate proportional increase to the dose rates themselves.

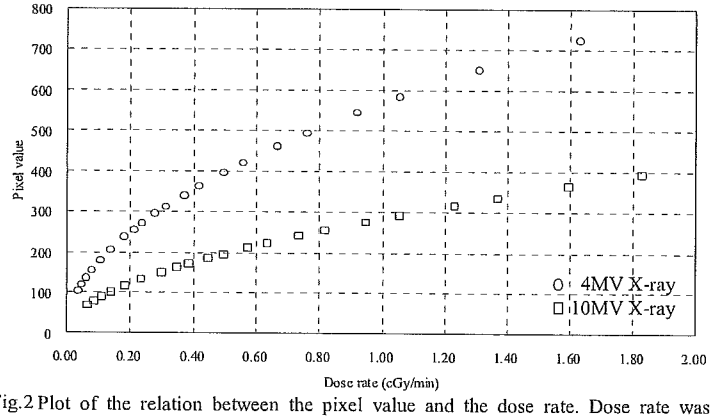

Fig.2 Plot of the relation between the pixel value and the dose rate. Dose rate was determined with the farmer type cylindrical ionization chamber on the central axis at the maximum depth for a 10 cm × 10 cm field size and 100 cm SOD with 4 MV (circle) and 10 MV X-rays (square). Pixel values were averaged over 11 × 11 pixels around the center of the field.

The results presented in this study were in good agreement with those reported by Essers et al.[8]. The relationship between pixel values and dose rates regressed as the secondary formula to the square root of the dose rates. Approximate formulas at 4 MV and 10 MV are shown in Eqs. (3) and (4), respectively.

$$P = 3.2381D + 569.08\sqrt{D} - 5.5168 \qquad R^2 = 1.0000 \qquad (3)$$

$$P = 22.085D + 260.32\sqrt{D} + 0.1266 \qquad R^2 = 1.0000 \qquad (4)$$

P: pixel value, D: dose rate (cGy/min), R^2: coefficient of determination.

From these results, the abovementioned formulas were considered to be a good tool for calculation of EPID doses from the measured pixel values.

C. Effects of scattered radiation

Fig. 4 shows the EPID doses with respect to the changes in the size of the irradiation field. EPID doses showed a marked increase till the area of the irradiation field was increased to 12 cm × 12 cm, while the increase was gradual when the area of the irradiation field was increased above that. Fig. 5 indicates the total scatter correction factor (*Sc,p*) obtained from data of the EPID and the farmer type cylindrical ionization chamber at 4 MV. There was a tendency for the *Sc,p* value of EPID dose to increase with field size in comparison with that from the farmer type cylindrical ionization chamber. *Sc,p* values from the EPID were higher by 1.2% than those from the farmer type cylindrical ionization chamber for a 20 cm × 20 cm area irradiation field and were higher by less than 1% for a 15 cm × 15 cm area irradiation field. On the other hand, for the irradiation of 10 MV, the opposite phenomena was observed, i.e., *Sc,p* values from the EPID decreased. The values from the EPID were 0.8% lower and less than 0.2% of those from the farmer-type cylindrical ionization chamber for a 4 cm × 4 cm area irradiation field and other field sizes, respectively.

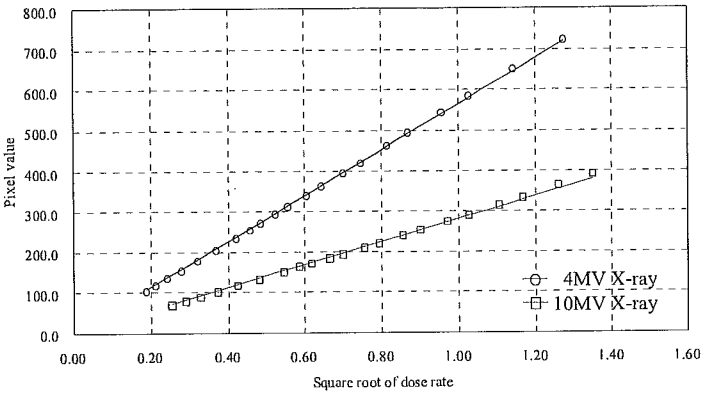

Fig.3 Plot of the relation between pixel values and the square root of the dose rate. Dose rate was determined with the farmer type cylindrical ionization chamber on the central axis at the maximum depth for a 10 cm × 10 cm field size and 100 cm SOD with 4 MV (circle) and 10 MV X-rays (square). The solid line represents an approximate value according to Van Herk's theory 10). Pixel values were averaged over 11 × 11 pixels around the center of the field.

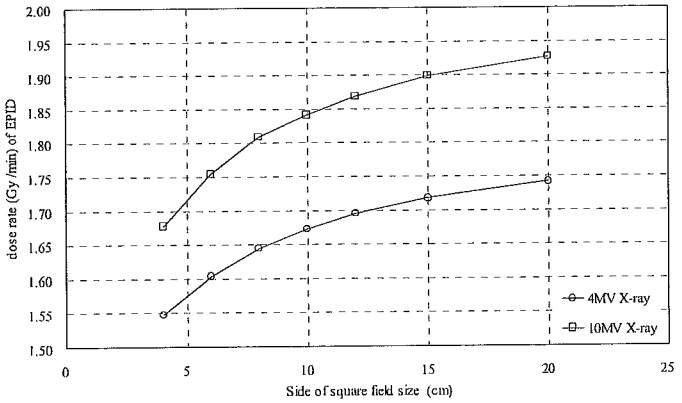

Fig.4 EPID dose rates obtained from pixel values of the field sizes from 4 cm × 4 cm to 20 cm × 20 cm. The measurements were done at the maximum depth on the central axis for a 100 cm SOD with 4 MV and 10 MV X-rays. Pixel values were averaged over 11 × 11 pixels around the center of the field.

IV. DISCUSSION

It was considered, based on the results, that when the collection interval was short, the pixel values increased, and when it was long, few increments in pixel value occurred. Therefore, an interval of over 30 s was considered to be a good condition for image collection. With

respect to the ionizing phenomenon, it was suggested that electric charges in the liquid ionizing chamber of L-EPID were almost saturated at a collection interval of more than 30 s, but some electric charges remained when the collection interval was shorter.

It was speculated that the causes of pixel value deviations between the first image and other images included in each collection Group are the changes in temperature within ionizing chambers according to the voltage supply to the L-EPID.

Stable pixel values independent of the cumulative irradiation dose are required for precise dosimetric verification, since small differences of pixel value as mentioned above lead to large ones in the converted EPID dose. L-EPID images should be collected under a suitable condition wherein few pixel values are affected by residual electric charge.

As described by Van Herk[10], the relationship between pixel values and dose rates indicated that the pixel values were approximately proportional to the square root of the dose rates. However, we observed that pixel values increased gradually, when X-ray dose exceeded 0.5 Gy/min (Fig. 2). In the case of irradiation less than 0.5 Gy/min using 4 MV or 10 MV X-rays, the pixel values had an approximately proportional increase to the square root of the dose rates. For an irradiation of more than 0.5 Gy/min, pixel values showed an approximate proportional increase with the dose rates. This result led us to consider that the theory described by Van Herk[10] required modification. We propose a new improved formula for Eq. (1) in our hypothesis, as follows.

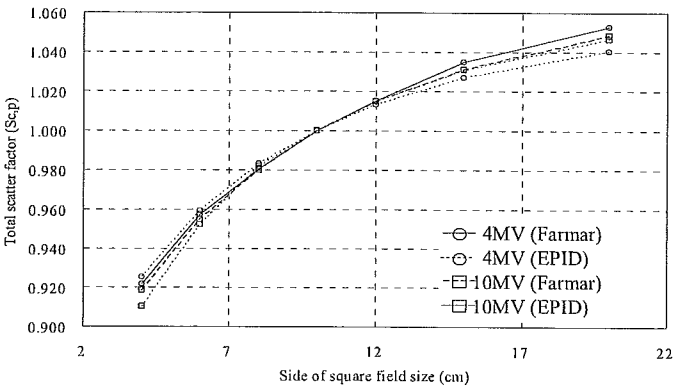

Fig.5 The total scatter factor (Sc,p) of the dose rates obtained from pixel values of the EPID and the farmer type cylindrical ionization chamber. The measurements were done at the maximum depth on the central axis for a 100 cm SOD with 4 MV and 10 MV X-rays. The dose rates were normalized to 1.0 for 10 cm × 10 cm field sizes. Pixel values were averaged over 11 × 11 pixels around the center of the field.

In sequential acquisition of L-EPID images, it was assumed that there were three phenomena: (1) the generation of new ion pairs balances the loss of ion pairs caused by the ion recombination; (2) the generation of new ion pairs exceeds loss of ion pairs caused by the ion recombination; and (3) fluctuation of sensitivity of the liquid ionizing chamber occurs with setup conditions for image collection.

In an irradiation process over a substantial length of time, the added concentration of ion pairs by generation and recombination should be considered. Moreover, a correction term for sensitivity, C, is

required. Therefore, the measured final concentration of ion pairs, N_{final} is expressed as follows.

$$N_{final} = n_{eq} + \frac{dn(t)}{dt} + c$$
$$= \sqrt{\frac{N_{in}}{\alpha}} + \left\{ N_{in}(t) - \alpha n(t)^2 + C \right\} \quad (5)$$

where C is constant. For N_{in} to be equal to $\beta \cdot D$, Eq. (5) can be converted to the following secondary formula with respect to the square root of the dose rates.

$$N_{final} = \beta \cdot D + \sqrt{\frac{\beta}{\alpha} \cdot D} - \alpha n(t)^2 + C \quad (6)$$

Then, as the relation between pixel value, (P) and concentration of ion pairs is $P = \gamma \cdot N_{final}$, Eq. (6) can be changed to Eq. (7).

$$P = a \cdot D + b \cdot \sqrt{D} - h \quad (7)$$

Here, a and b are constants, h is the constant for loss of ion pairs caused by ion recombination and for the sensitivity correction factor of ionizing chambers. Hence, $h = \gamma(\cdot\alpha \cdot n(t)^2 + C)$. The relationship between the pixel values and the dose rates in Eq. (7) can be given as a secondary dimension quantic formula the same as the approximate Eq. (3), (4) as above mentioned.

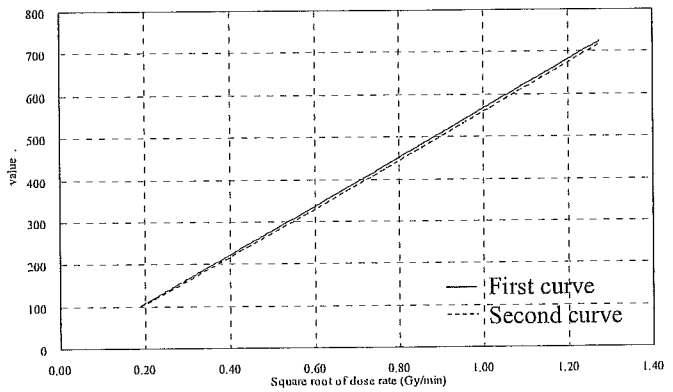

Fig.6 Plot of the relation between the pixel values and the square roots of the dose rates determined using the farmer type cylindrical ionization chamber on the central axis at maximum depth for field size (10 cm × 10 cm) and SOD (100 cm) with 4 MV X-rays. The second curve was determined 14 days after the first curve. Pixel values were averaged over 11 × 11 pixels around the center of the field.

The characteristic curve of the pixel values from the EPID at 4 MV were rearranged (Fig. 6) for assessment of the sensitivity correction factor (h). The obtained curve indicated that sensitivities of the pixels decreased. The pixel values decreased 1.1% similar to the daily changes mentioned above. However, EPID doses showed 5.5% and 3.8% decreases in high dose and low dose regions, respectively. The values in this study were in good agreement with those reported by Zhu et al[14].

When we multiplied h by 2.47, the difference in the EPID dose rate was within ±0.1%. We, now,

introduce a constant (k) as a correction factor for the daily deviation of the sensitivity of the ionizing chamber.

According to the consideration, formula (7) was changed as follows.

$$P = a \cdot D + b \cdot \sqrt{D} - k \cdot h \qquad (8)$$

Eq. (8) implies that the characteristic curve of the pixel values does not need to be constructed, we have to acquire k as a factor for the daily deviation from measurements in the standard irradiation field.

The effect of the scattered rays on sensitivity in the EPID was speculated to depend on the effects of the water equivalent materials and PCB in the front, back, and supports of the EPID structure. For 4 MV, the effects of the scattering body in the back were stronger than those for 10 MV, and the difference of Sc,p values between the L-EPID and farmer type cylindrical ionization chamber was considered to be high.

V. CONCLUSIONS

We quantified effects from contaminants and the sensitivity variation in the electric charge layer with the liquid ionization chamber EPID from the viewpoint of image collection setting. Further, we revised the theory presented by Van Herk[10] for the dose rate of L-EPID, which led to the following equation.

$$P = a \cdot D + b \cdot \sqrt{D} - k \cdot h$$

h: changes in effect from the contaminant concentration in electric charge layer, k: sensitivity correction factor of daily deviation.

By using this formula, the obtained pixel values were converted into the dose rates within ±0.1% errors.

ACKNOWLEDGMENTS

We thank Professor Masao Hoshina, Department of Radiology, Gunma Prefecture College of Health Science, and Dr. Jack Yang, Institute for Advanced Radiation Oncology, Monmouth Medical Center for useful discussions and advice.

REFERENCES

1) Boyer AL, Antonuk L, Fenster A et al.: A review of electronic portal imaging devices (EPIDs). Med. Phys. 19: 1-16, 1992

2) Meertens, Van Herk M, Bijhold J and Bartelink H: First clinical experience with a newly developed electronic portal imaging device. Int. J. Radiat. Oncol. Biol. Phys. 18: 1173-1182, 1990

3) Gilhuijs KAG, Touw A, Van Herk M and Vijlbrief RE: Optimization of automatic portal image analysis. Med. Phys. 22: 1089-1099, 1995

4) Ruden BI: Evaluation of the clinical use of TLD. Acta. Radiol. Ther. Phys. Biol. 15: 447-464, 1976

5) Eunens G, Van Dam J, Dutreix A and Van der Schueren E: Quality assurance in radiotherapy in vivo dosimetry. 1. Entrance dose measurement, a reliable procedure. Radiother. Oncol. 22: 285-289, 1991

6) An Dam J, Vaerman C, Blancket N et al.: Are port films reliable for in vivo exit dose measurement?. Radiother. Oncol. 25: 67-72, 1992.

7) Fiorino C, Del Vacchio A, Cattaneo GM et al.: Exit dose measurement by portal film dosimetry. Radiother. Oncol. 29: 336-340, 1993.

8) Essers M, Hoogervorst BR, Van Herk M, et al.: Dosimetric characteristics of a liquid filled electronic portal imaging device. Int. J. Radiat. Oncol. Biol. Phys. 33: 1265-1272 , 1995

9) Yin FF, Schell MC and Rubin P: Input/output characteristics of a matrix ion-chamber electronic portal imaging device. Med. Phys. 2: 1447-1454, 1994

10) Van Herk M: Physical aspects of a liquid-filled ionization chamber with pulsed polarizing voltage. Med. Phys. 18: 692-702. 1991

11) Kirby MC and Williams PC: Measurement possibilities using an electronic portal imaging device. Radiother. Oncol. 29: 237-243, 1993

12) Heijment BJM, Pasma KL, Kroonwijk M, et al.: Portal dose measurement in radiotherapy using an electronic portal imaging device (EPID). Phys. Med. Biol. 40: 1943-1955, 1995

13) Essers M, Boellaard R, Van Herk M, et al.: Transmission dosimetry with a liquid filled electronic portal imaging device: Int. J. Radiat. Oncol. Biol. Phys. 34: 931-941, 1996

14) Zhu YZ, Jiang XQ and Van Dyk J: Portal dosimetry using a liquid ion chamber - dose response studies. Med. Phys. 22: 1101-1106, 1995

15) Curtin-Savard AJ and Podgorsak EB: An electronic portal imaging device as a physics tool. Med. Dosimetry 22: 101-105, 1997

16) Curtin-Savard AJ and Podgorsak EB: Verification of segmented beam delivery using a commercial electronic portal imaging device. Med. Phys. 26: 737-742, 1999

Analysis of Local Control in Patients with Non-Hodgkin's Lymphoma According to the WHO Classification

Koh-ichi Sakata[1], Masaaki Satoh[2], Masanori Someya[1], Hisayasu Nagakura[1], Atushi Oouchi[1], Kensei Nakata[1], Katsuhisa Kogawa[3], Kazumitsu Koito[1], Masato Hareyama[1], Tetsuo Himi[4]

Purpose: To analyze the influence of radiotherapy doses, chemotherapy doses, and clinical parameters on in-field disease control to assess the optimal radiation doses for treatment of non-Hodgkin's lymphoma according to the newly proposed WHO classification.

Patients and Methods: Subjects consisted of 35 extranodal marginal-zone B-cell lymphomas of mucosa-associated lymphoid tissue (MALT) type, 75 diffuse large B-cell lymphomas (DLBCL), 14 follicular lymphomas, 17 extranodal natural killer (NK)/T-cell lymphomas, nasal type, eight unclassified peripheral T-cell lymphomas, four anaplastic large-cell lymphomas, T/null cell type, and five others. 59 patients received radiotherapy alone. 98 patients received CHOP, modified CHOP, or more intensive chemotherapy, and six patients were treated with other combination.

Results: No patients with MALT lymphoma had in-field local recurrence. There were no recurrences in DLBCL patients who received chemotherapy in which the doses of adriamycin were > 200 mg/m^2, nor in DLBCL patients who were treated with > 45 Gy. Only nine of 15 patients with T-cell lymphoma treated with ≤ 50 Gy and three of five patients treated with > 50 Gy had local control. The dose of adriamycin had no influence on local control of T-cell lymphoma.

Conclusion: T/NK-cell lymphomas were more radioresistant than B-cell lymphomas. The prognosis for peripheral T/NK-cell lymphomas is poor even when treated by irradiation combined with chemotherapy.

Key Words: Non-Hodgkin's lymphoma · WHO classification · T-cell lymphoma · Dose-response analysis

Strahlenther Onkol 2005;181:385–91
DOI 10.1007/s00066-005-1330-x

Analyse der lokalen Kontrolle beim Non-Hodgkin-Lymphom gemäß WHO-Klassifikation

Ziel: Untersuchung des Einflusses der Strahlungsdosis, Chemotherapie-Intensität und klinischer Parameter auf die Kontrolle lokalisierter Herde, um optimale Parameter für die Behandlung des Non-Hodgkin-Lymphoms gemäß der vor kurzem vorgeschlagenen WHO-Klassifikation zu ermitteln.

Patienten und Methodik: In die Untersuchung einbezogen wurden 35 extranodale („marginal-zone") B-Zell-Lymphome des Mukosa-assoziierten-Lymphom-(MALT-)Typs, 75 diffuse großzellige B-Zell-Lymphome (DLBCL), 14 follikuläre Lymphome, 17 extranodale Natürliche-Killer-(NK-)/T-Zell-Lymphome (Nasaltyp), 8 unklassifizierte periphere T-Zell-Lymphome, 4 anaplastische (großzellige) Lymphome (T/null-Zell-Typ) and 5 andere. 59 Patienten erhielten ausschließlich Strahlentherapie. 98 Patienten erhielten CHOP, CHOP modifiziert oder eine intensivierte Chemotherapie, und 6 Patienten wurden mit einer anderen Kombination behandelt.

Ergebnisse: Bei keinem der MALT-Lymphom-Patienten kam es zu einem Lokalrezidiv. Rezidive traten weder bei DLBCL-Patienten auf, die Chemotherapie mit Adriamycin in Dosierungen > 200 mg/m^2 erhalten hatten, noch bei DLBCL-Patienten, die mit > 45 Gy behandelt worden waren. Nur bei 9 von 15 T-Zell-Lymphom-Patienten, die mit ≤ 50 Gy, und bei 3 von 5 Patienten die mit > 50 Gy behandelt worden waren, wurde eine lokale Kontrolle erreicht. Die Adriamycin-Dosis beeinflusste die lokale Kontrolle von T-Zell-Lymphomen nicht.

Schlussfolgerungen: T/NK-Zell-Lymphome zeigten sich strahlungsresistenter als B-Zell-Lymphome. Die Prognose peripherer T/NK-Zell-Lymphome ist selbst bei Kombination von Strahlen- und Chemotherapie schlecht.

Schlüsselwörter: Non-Hodgkin-Lymphom · WHO-Klassifikation · T-Zell-Lymphom · Dosis-Wirkungs-Analyse

[1] Department of Radiology, Sapporo Medical University, School of Medicine, Sapporo, Japan,
[2] Department of Clinical Pathology, Sapporo Medical University, School of Medicine, Sapporo, Japan,
[3] Department of Fourth Internal Medicine, Sapporo Medical University, School of Medicine, Sapporo, Japan,
[4] Department of Otorhinolaryngology, Sapporo Medical University, School of Medicine, Sapporo, Japan.

Received: June 8, 2004; accepted: February 17, 2005

Introduction

The clinical course of non-Hodgkin's lymphoma (NHL) is highly variable, depending on the histological subtype and primary site of organ involvement [20]. Therefore, therapy should be tailored to the individual patient, taking these patient-to-patient differences into account.

With advances in combination chemotherapy regimens, patients with intermediate or more aggressive NHL are usually treated with combined chemotherapy and irradiation [3, 13, 19].

However, little information is available on the optimal radiotherapy dose necessary to achieve in-field disease control and prolonged relapse-free survival in patients with NHL who receive chemotherapy. Although no prospective randomized studies have been performed to evaluate the optimal radiotherapy dose for NHL, some retrospective data support the use of lower radiotherapy doses for low-grade lymphoma [17]. For intermediate/high-grade lymphoma, the radiation dose issue is less clear, but higher doses may be needed [17, 29]. Besides, most of the dose-response analyses of lymphoma in the literature were performed in the era when patients received radiotherapy alone [4, 12, 28].

The Revised European and American Lymphoma (REAL) classification and the WHO classification were proposed and have been rapidly accepted [10, 11, 22, 25]. These classifications were proposed based on the cell of origin and delineate individual disease entities from the perspective of morphological features, immunophenotype and/or stage of differentiation, genotype, etiology, epidemiology, and clinical behavior. Therefore, it is expected that radiation doses and fields suitable for avoidance of unnecessary irradiation of critical organs can be selected by adhering to the WHO classification. However, many studies, including our previous one [26] employed the Working Formulation. Thus, there is only limited information on the clinical characteristics of NHL from the perspective of the WHO classification.

We reevaluated histopathologic specimens of NHL, using the WHO classification, and investigated the relationship between the clinical characteristics and histopathologic classification of these specimens, in order to assess the usefulness of this new classification system in selecting treatment modalities. We also analyzed the influence of radiotherapy doses as well as other treatment-related and clinical parameters on in-field disease control in order to assess the optimal radiation doses for treatment of NHL according to the WHO classification.

Patients and Methods

Patient Characteristics

Between 1983 and 2001, 158 patients with histologically confirmed NHL were treated at the Department of Radiology, Sapporo Medical University Hospital, Japan. Their characteristics are summarized in Table 1.

There were 35 extranodal marginal-zone B-cell lymphomas of mucosa-associated lymphoid tissue (MALT) type (MALT lymphoma), 75 diffuse large B-cell lymphomas (DLBCL), 14 follicular lymphomas (five for grade 1, six for grade 2, and three for grade 3), 17 extranodal natural killer (NK)/T-cell lymphomas, nasal type (nasal NK/T-cell lymphoma), eight unclassified peripheral T-cell lymphomas, four anaplastic large-cell lymphomas, T/null cell type, and five others. Nasal NK/T-cell lymphoma is more prevalent in the younger generation, compared with the other lymphomas. These patients included 94 with stage I, 45 with stage II, ten with stage III, and nine with stage IV disease.

Table 2 shows the histopathologic distribution according to primary sites. Most MALT lymphomas originated from the orbit (29 patients) or thyroid gland (three patients). Of the eight peripheral T-cell lymphomas, four originated in the nasal cavity, and two in the lymph nodes. Nasal NK/T-cell lymphomas were only seen in the nasal sinus. DLBCLs were all from primary sites.

Table 1. Patient characteristics. ADM: adriamycin; DLBCL: diffuse large B-cell lymphoma; NK-cell: natural killer cell.

Tabelle 1. Patientencharakteristika. ADM: Adriamycin; DLBCL: diffuses großzelliges B-Zell-Lymphom; NK-cell: Natürliche Killer-Zelle.

	MALT lymphoma	DLBCL	Follicular lymphoma	Peripheral T/NK-cell lymphoma	Anaplastic large-cell lymphoma	Nasal NK/T-cell lymphoma
Male : female ratio	16 : 19	41 : 34	7 : 7	5 : 3	0 : 4	10 : 7
Average age (years)	61.9	60.8	57.0	51.1	56.0	53.5
Radiation dose (Gy)						
• Median	44	44	44	46	45	50
• Range	30–50	30–60	40–50	40–58	40–50	30–74
Chemotherapy (n)						
• No	23	22	10	1	1	2
• Not including ADM	0	2	0	2	0	2
• CHOP, modified CHOP or more intensive	22	51	4	5	3	13
Stage I (n)	30	35	8	6	1	11
Stage II (n)	3	29	4		3	4
Stage III or IV (n)	2	11	2	2		2

Histology and T/B-Phenotype

One of the authors (M.Sa.), without knowledge of clinical information on individual patients, reassessed specimens using the morphological and immunologic techniques described below. Histological classification was performed according to the WHO classification [10]. Immunohistochemical studies were performed using paraffin sections, the avidin-biotin peroxidase complex technique, and a panel of monoclonal antibodies (L2 CD3, MT1, UCHL1, and CD56).

Treatment (Table 1)

59 patients received radiotherapy alone. Radiation therapy was usually delivered to the involved field. In patients receiving chemotherapy and subsequent irradiation, the radiation field was set for primary sizes of lesions. The dose per fraction ranged from 1.8 to 2.0 Gy. All treatment regimens included five daily fractions per week.

98 patients received CHOP (cyclophosphamide: 750 mg/m^2 or 600 mg/m^2 in the elderly; adriamycin: 50 mg/m^2 or 40 mg/m^2 in the elderly; vincristine: 1.4 mg/m^2; and prednisolone: 60 mg for 5 days), modified CHOP, or more intensive chemotherapy, and six patients were treated with other combination- or single-agent chemotherapy, mostly before irradiation.

Statistical Analysis

In-field failure was defined as any failure with an in-field component, i.e., any recurrence in the irradiated volume. The living patients whose follow-up periods were < 24 months were excluded from this analysis.

The overall and failure-free survival rates were calculated from the start of treatment by the Kaplan-Meier method, and differences in the survival rates were examined by the log-rank test. Failure-free status was scored at the time when the last systemic evaluation of the patients was performed. The median follow-up for the living patients was 60 months.

Results

In our study, the overall and relapse-free survival rate for DLBCL patients with brain as the primary site was poor. DLBCL patients with brain primary also demonstrated lower relapse-free survival rates than patients with Waldeyer's ring primary (data not shown). According to these results and others [21], primary brain lymphomas were excluded from the following analysis, because their natural history and prognosis are very different from the other lymphomas [6].

Figure 1a shows overall survival rates of stage I and stage II patients according to histological classification. The overall 5-year survival rate for patients with MALT lymphoma was 100%. Patients with MALT lymphoma demonstrated higher

Table 2. Primary sites and pathologic classification. DLBCL: diffuse large B-cell lymphoma; L/N: lymph nodes; MALT: mucosa-associated lymphoid tissue; NC: nasal cavity; NK-cell: natural killer cell; NP: nasopharynx; PS: paranasal sinus; SG: salivary glands; WR: Waldeyer's ring.

Tabelle 2. Primärmanifestation und histopathologische Klassifizierung. DLBCL: diffuses großzelliges B-Zell-Lymphom; L/N: Lymphknoten; MALT: Mukosa-assoziiertes lymphoides Gewebe; NC: Nasenhöhle; NK-cell: Natürliche Killer-Zelle. NP: Nasopharynx; PS: Paranasalsinus; SG: Speicheldrüsen; WR: Waldeyer-Ring.

Pathology	Brain	Orbit	NC	PS	NP	WR	Thyroid	SG	L/N	Others
MALT lymphoma		29					3	2		1
DLBCL	7	3	4	4	6	31	1	1	15	3
Follicular lymphoma		3				2		3	5	1
Peripheral T/NK-cell lymphoma			4			1			2	1
Anaplastic large-cell lymphoma	1		1			1				1
Nasal NK/T-cell lymphoma			17							

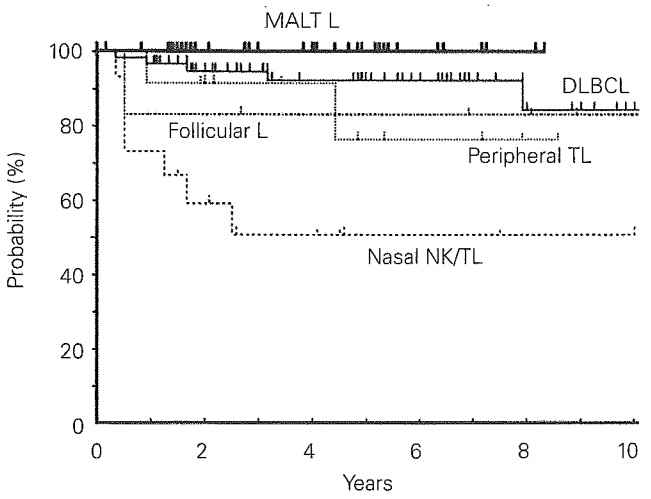

Figure 1a – Abbildung 1a

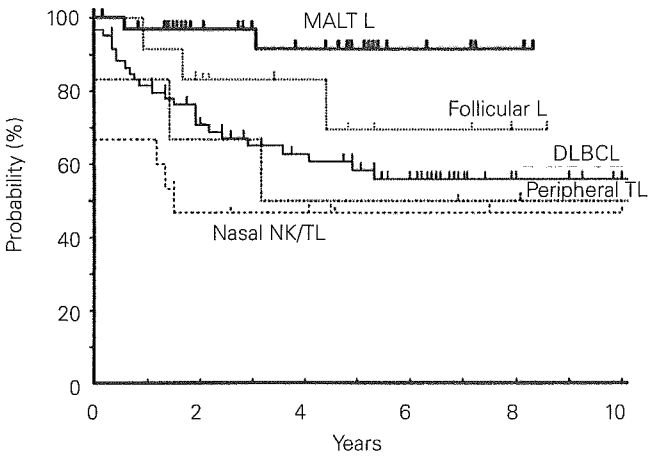

Figure 1b – Abbildung 1b

Figures 1a and 1b. Overall survival curves (a) and relapse-free survival curves (b) for patients with stage I and II non-Hodgkin's lymphoma according to histological examinations. DLBCL: diffuse large B-cell lymphoma; L: lymphoma; MALT: mucosa-associated lymphoid tissue; Nasal NK/TL: nasal natural killer/T-cell lymphoma; Peripheral TL: unclassified peripheral T-cell lymphomas.

Abbildungen 1a und 1b. Gesamtüberleben (a) und rezidivfreies Überleben (b) bei Patienten mit histologisch gesichertem Non-Hodgkin-Lymphom Stadium I und II. DLBCL: diffuses großzelliges B-Zell-Lymphom; L: Lymphom; MALT: Mukosa-assoziiertes lymphoides Gewebe; Nasal NK/TL: nasales Natürliche-Killer/T-Zellen-Lymphom; Peripheral TL: nicht klassifizierte periphere T-Zell-Lymphome.